Atomisation and Spray Technology **3** (1987) 309–337

Modeling Atomization Processes in High-Pressure Vaporizing Sprays

Rolf D. Reitz

Fluid Mechanics Department, General Motors Research Laboratories, Warren, Michigan 48090–9057, USA

(Received 2 September 1987; accepted after revision 1 October 1987)

ABSTRACT

A multi-dimensional computer model is used to study atomization and vaporization of a liquid jet injected from a round hole into a compressed gas. Atomization is described using a new method whereby 'blobs' are injected (with sizes equal to the nozzle exit diameter), and breakup of the blobs and the resulting drops is modeled using a stability analysis for liquid jets. This method can also predict various regimes of breakup which result from the action of different combinations of liquid inertia, surface tension and aerodynamic forces on the jet. The product drops are distinguished from the parent drop by having different dropsizes (previous drop breakup models have lumped the parent and product drops together). This has a significant effect on the fuel vapor distribution in a high-pressure spray because the small product drops vaporize rapidly. Like existing models, the model accounts for drop collision and coalescence, and the effect of drops on the gas turbulence. These effects are important in high-pressure sprays where breakup of the liquid yields a core region near the nozzle containing large drops. Fuel vaporization in the core is found to depend strongly on the atomization details near the nozzle. Downstream of the core, fuel–air mixing is found to be determined by a competition between local drop breakup, coalescence and vaporization rates.

LIST OF NOTATIONS

a liquid jet or blob radius

A_1 spray angle constant, eqn (7)

Atomisation and Spray Technology 0266-3481/87/$03·50

A_2 dropsize constant, eqn (8)
A_3 breakup length constant, eqn (9)
b collision impact parameter, eqn (18)
B mass transfer number $(Y_{surf} - Y)/(1 - Y)$
B_0 dropsize constant, eqn (10)
B_1 breakup time constant, eqn (12)
c nozzle coefficient of discharge
$C_{1,2}$ constants of integration in stability analysis
C_D drop drag $= 12(1 + 0{\cdot}26\,\mathrm{Re}_2^{0.67})/\mathrm{Re}_2$, $\mathrm{Re}_2 < 500$
$= 0.424$, $\mathrm{Re}_2 \geq 500$
d_0 nozzle exit diameter = 2a
D drop diameter, mass diffusivity
F drop acceleration, eqn (20)
i $\sqrt{-1}$
I_n nth order modified Bessel function of the first kind
k wavenumber $2\pi/\lambda$, turbulence kinetic energy
K_n nth order modified Bessel function of the second kind
L core length, eqn (9)
N number of drops
Nu Nusselt number $(2{\cdot}0 + 0{\cdot}85\,\mathrm{Re}_2^{0.5}(\nu_2/a)^{0.33})\ 1n(1 + B)/B$
p pressure, probability
q random number uniform on interval [0,1]
r radial coordinate, drop radius
Re Reynolds number Wa/ν
S turbulence energy source term, eqn (19)
Sh Sherwood number $(2{\cdot}0 + 0{\cdot}85\,\mathrm{Re}_2^{0.5}(\nu_2/D)^{0.33})\ 1n(1 + B)/B$
t time
T Taylor parameter $Z\,We_2^{0.5}$, breakup time
u axial velocity component, gas fluctuating velocity vector
U jet exit velocity, gas velocity vector
v radial velocity component, drop velocity vector
W relative velocity vector between liquid and gas
We Weber number $\rho W^2 a/\sigma$
Y mass fraction of fuel vapor
z axial coordinate
Z Ohnesorge number $\nu_1(\rho_1/\sigma a)^{0.5}$
$\mathscr{L}$ wavenumber $\sqrt{(k^2 + \omega/\nu_1)}$
$\mathscr{R}$ real part of a complex quantity

α thermal diffusivity
γ coalescence parameter r_1/r_2
ΔP effective injection pressure $P_1 - P_2$

Δt numerical time step
ε rate of dissipation of turbulence kinetic energy
η surface wave amplitude
θ, Θ jet divergence or spray angle
λ wavelength
Λ wavelength of fastest growing wave
ν dynamic viscosity, collision frequency
ρ fluid density
σ surface tension coefficient
τ liquid breakup time
ϕ velocity potential
ψ stream function
ω wave growth rate $=\mathcal{R}(\omega)$
Ω maximum wave growth rate

Subscripts
0 initial value
1 liquid phase, first
2 gas phase, second
3, 2 Sauter Mean
surf surface value

1 INTRODUCTION

The dispersion of spray drops in a gas is important in many industrial processes in order to bring about efficient mass and heat transfer between liquid and gas phases. In engine applications, the need for an improved understanding of fuel sprays is emphasized by the fact that injector performance is known to affect engine operation. One of the key processes affecting spray behavior is atomization, the process whereby the injected liquid is broken into drops. The regimes of atomization of interest in engines are reviewed by Reitz and Bracco.[1,2] In spite of the importance of atomization, the mechanisms of liquid breakup are still not well understood, even for the relatively simple case of a constant pressure injection from a single hole nozzle into a high density gas. This type of injection gives a conical spray whose divergence starts at the nozzle. There is uncertainty about the inner structure of the spray since experimental measurements are complicated by the dense spray which obscures the breakup details.

Fortunately computational techniques are now available to help characterize sprays. In the present work, a recently developed multi-

dimensional engine combustion computer code called KIVA was applied to study spray processes in high-pressure vaporizing sprays. The code computes interactions between spray drops and the gas, accounts for the phenomena of drop breakup, drop collision and coalescence, and for the effect of drops on the gas turbulence. This study considers sprays in a relatively simple well-defined environment (unconfined spray with initially quiescent gas, constant gas and liquid pressures, single component fuel) for which experimental data are available. Further work is needed to address other processes also relevant to engines (e.g. multi-component-fuel vaporization, drop-wall interactions, spray combustion, soot and radiation). As such, the present study is a step toward the development and validation of a general, predictive, engine combustion model.

The atomization process is not resolved by the code. This is because atomization occurs on time and length scales too short to be resolved with practical computational grid sizes and time steps. Instead, atomization is modeled as a sub-grid-scale process. (For example, in a diesel engine with injection velocity 300 m/s and nozzle hole diameter 0.2 mm, the atomizing jet moves a distance equal to its diameter in 0·6 μs and the dropsizes are below 50 μm. Present supercomputer storage and run times limit 3-D engine simulations to grid sizes >1 mm and time steps >1 μs.)

Similar considerations apply also to other drop and gas processes which occur on scales below the resolution of the grid (e.g. drop breakup, drop collision and coalescence, turbulence and the dispersion of drops by turbulence, and vaporization) and submodels are used for these phenomena. The use of a submodel to describe an unresolved physical process necessarily introduces some empiricism into the computations. However, the compromise between accuracy and feasibility of computation is justified by the insight which model calculations offer. Confidence in model predictions and knowledge of their limitations is gained by comparison with experiments.

A new model for atomization is presented in the present study. The model uses the concept introduced by Reitz and Diwakar[3] that atomization of the injected liquid and the subsequent breakup of drops are indistinguishable processes within a dense spray. In the model of Reitz and Diwakar[3] the liquid is injected as discrete parcels of drops or 'blobs'. The injected drop's size decreases with time due to breakup and the size is specified using experimental drop breakup correlations. In the present study, new parcels containing product drops are added to the computation as the blobs break up, and the product drops themselves can undergo further breakups. The size of the product drops

is determined from the wavelength of unstable waves on the surface of the blobs.

The model of Reitz and Diwakar[3] predicts a core region near the nozzle which contains large drops, and the length of the core agrees with core length measurements in dense sprays. However, large drops vaporize slowly and that model predicts negligible vaporized fuel in the core region. This disagrees with recent fuel vapor measurements. The present atomization model predicts that small product drops co-exist with the large core drops. These small product drops vaporize rapidly and this leads to computed fuel vapor distributions near the nozzle that agree well with the vapor measurements.

Organization of the paper is as follows. First, a brief review is given of the jet stability analysis which is used later to formulate the new liquid breakup model. This analysis also introduces various regimes of breakup of liquid jets. Next, the KIVA code and its numerical methods are summarized. Following this, the submodels are described, starting with the models for liquid injection and atomization. It will be seen that the new liquid breakup model is quite general in that it recovers previous drop breakup models as limiting cases. Finally, the code is applied to compute regimes of jet breakup and to predict the structure and vaporization of high-pressure sprays.

2 JET STABILITY ANALYSIS AND BREAKUP REGIMES

The stability analysis is described in detail in Reitz and Bracco.[1] The analysis examines the stability of a cylindrical liquid surface to perturbations using a first order linear theory. The analysis starts by imposing on the surface an infinitesimal axisymmetric displacement of the form (see Fig. 1)

$$\eta = \mathcal{R}(\eta_0 e^{ikz+\omega t}) \tag{1}$$

and this ultimately leads to a dispersion equation, eqn (3) below. Equation (3) relates the growth rate, ω, of an initial perturbation of infinitesimal amplitude, η_0, to its wavelength λ (wavenumber $k = 2\pi/\lambda$). The relationship also includes the physical and dynamical parameters of the liquid jet and the surrounding gas.

Equation (3) is derived from the linearized hydrodynamical equations for the liquid and gas. The liquid equations are solved with wave solutions of the form $\phi_1 = C_1 I_0(kr)\exp(ikz + \omega t)$ and $\psi_1 = C_2 r I_1(\mathcal{L}r)\exp(ikz + \omega t)$. ψ_1 and ϕ_1 are the stream function and velocity potential, C_1 and C_2 are integration constants, $\mathcal{L}^2 = k^2 + \omega/\nu_1$, ν_1 is the

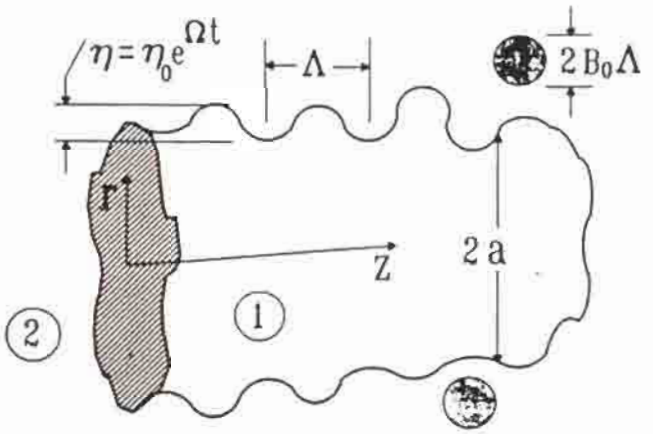

Fig. 1. Schematic diagram showing surface waves and breakup on a liquid blob. The surface wave growth rate is assumed to be that of the fastest growing wave ($\omega = \Omega$) of eqn (3). The corresponding wavelength is $\lambda = \Lambda$.

liquid dynamic viscosity and I_0 and I_1 are modified Bessel functions of the first kind. The liquid pressure is found from $p_1 = -\rho_1 \partial\phi_1/\partial t$ where ρ_1 is the liquid density (subscript 1 refers to liquid properties while subscript 2 identifies gas properties).

The gas equations of motion yield for the gas pressure at the interface $r = a$

$$p_2 = -\rho_2\left(W - i\frac{\omega}{k}\right)^2 k\eta \frac{K_0(ka)}{K_1(ka)}$$

when it is assumed that the gas is inviscid (K_0 and K_1 are modified Bessel functions of the second kind, and W is the relative velocity between the liquid and gas). With the assumption that $\eta \ll a$, the kinematic, tangential stress, and normal stress equations at the interface are

$$v_1 = \frac{\partial\eta}{\partial t}, \qquad \frac{\partial u_1}{\partial r} = -\frac{\partial v_1}{\partial z} \tag{2a, b}$$

$$-p_1 + 2\nu_1\rho_1 \frac{\partial v_1}{\partial r} - \frac{\sigma}{a^2}\left(\eta + a^2\frac{\partial^2\eta}{\partial z^2}\right) + p_2 = 0 \tag{2c}$$

(u_1, v_1 are the axial and radial liquid velocity components, and σ is the surface tension). Equations (2a, b) are used to eliminate C_1 and C_2, and when the velocity and pressure solutions are used in eqn (2c) one gets

the dispersion relationship

$$\omega^2 + 2\nu_1 k^2 \omega \left[\frac{I_1'(ka)}{I_0(ka)} - \frac{2k\mathscr{L}}{k^2 + \mathscr{L}^2} \frac{I_1(ka)}{I_0(ka)} \frac{I_1'}{I_1} \frac{(\mathscr{L}a)}{(\mathscr{L}a)} \right]$$

$$= \frac{\sigma k}{\rho_1 a^2} (1 - k^2 a^2) \left(\frac{\mathscr{L}^2 - k^2}{\mathscr{L}^2 + k^2} \right) \frac{I_1(ka)}{I_0(ka)}$$

$$+ \frac{\rho_2}{\rho_1} (W - i\omega/k)^2 k^2 \left(\frac{\mathscr{L}^2 - k^2}{\mathscr{L}^2 + k^2} \right) \frac{I_1(ka) K_0(ka)}{I_0(ka) K_1(ka)} \tag{3}$$

where the primes denote differentiation. Numerical solutions of eqn (3) indicate that there is a single maximum in the wave growth rate curve, $\omega = \omega(k)$.

For the present study it was convenient to generate curve-fits of numerical solutions to eqn (3) for the maximum growth rate ($\omega = \Omega$)

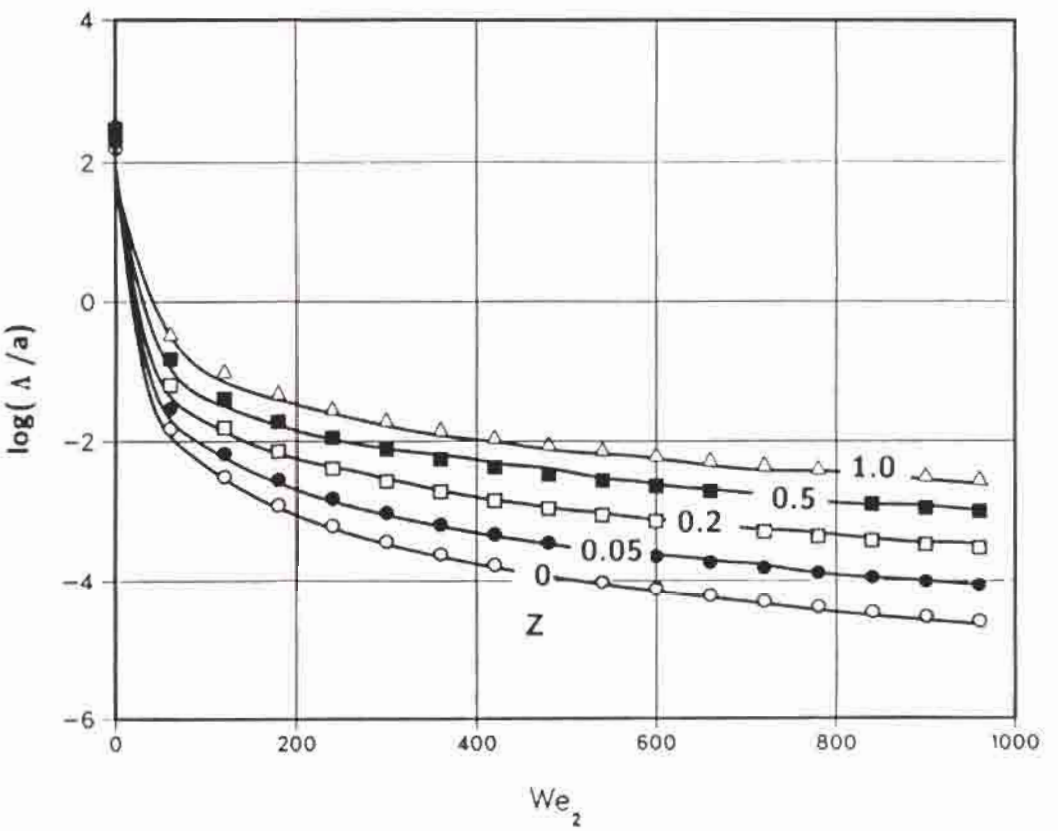

Fig. 2. Wavelength of the most unstable surface wave versus Weber number, We_2, as a function of Ohnesorge number, Z. Lines, numerical solutions of eqn (3); symbols, curvefit, eqn (4).

and for the corresponding wavelength ($\lambda = \Lambda$), viz.

$$\frac{\Lambda}{a} = 9{\cdot}02\,\frac{(1+0{\cdot}45Z^{0{\cdot}5})(1+0{\cdot}4T^{0{\cdot}7})}{(1+0{\cdot}87We_2^{1{\cdot}67})^{0{\cdot}6}} \tag{4}$$

$$\Omega\left[\frac{\rho_1 a^3}{\sigma}\right]^{0{\cdot}5} = \frac{(0{\cdot}34+0{\cdot}38We_2^{1{\cdot}5})}{(1+Z)(1+1{\cdot}4T^{0{\cdot}6})}. \tag{5}$$

Λ and Ω characterize the fastest growing (or most probable) wave on the liquid surface. Here, the Ohnesorge parameter $Z = We_1^{0{\cdot}5}/\mathrm{Re}_1$ and $T = Z\ \mathrm{We}_2^{0{\cdot}5}$. The Weber numbers are $\mathrm{We}_1 = \rho_1 W^2 a/\sigma$ and $\mathrm{We}_2 = \rho_2 W^2 a/\sigma$ and the Reynolds number is $\mathrm{Re}_1 = Wa/\nu_1$. Equations (4) and (5) are shown in Figs 2 and 3, and they represent numerical solutions to eqn (3) adequately for $Z \leq 1$ and for ρ_2/ρ_1 less than about 0·1. These conditions are typically satisfied for the sprays of interest here.

Equation (3) has been used by Reitz and Bracco[1] as a framework to organize jet breakup regimes. Examples of jets in four breakup regimes are shown in Fig. 4. At low gas Weber numbers, We_2, breakup is in the Rayleigh regime (Fig. 4(a)), and the dropsizes are larger than the jet

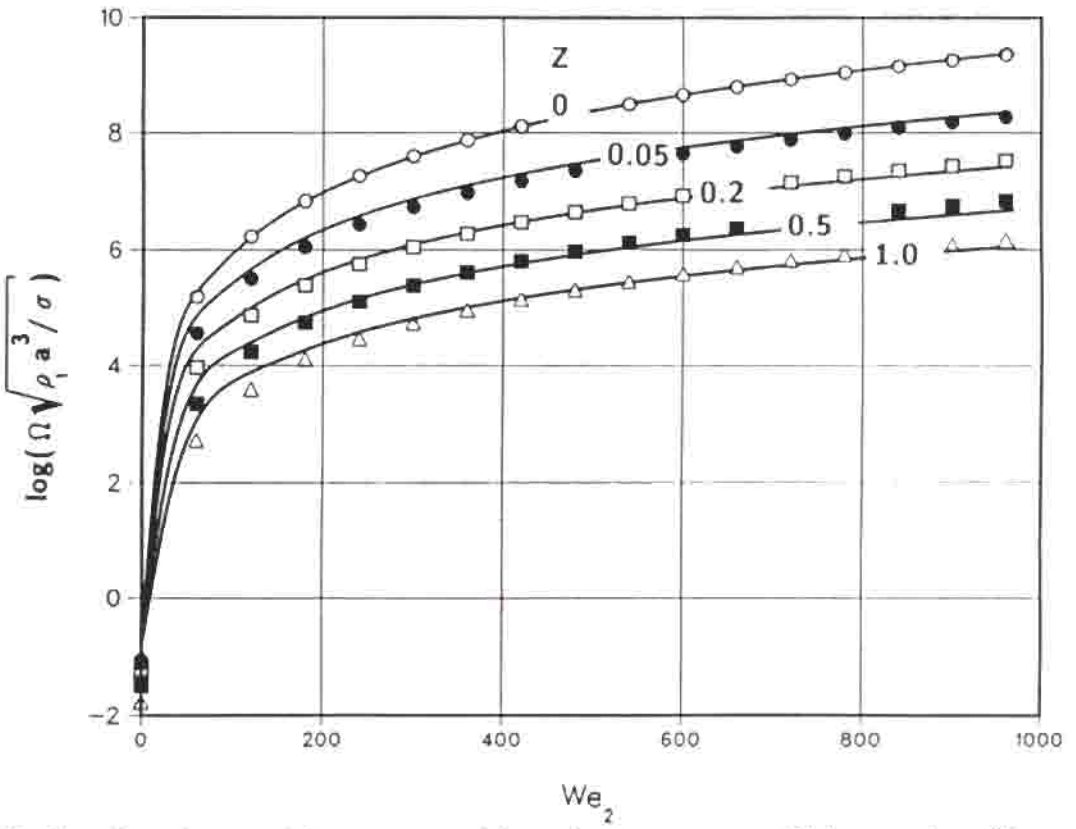

Fig. 3. Growth rate of the most unstable surface wave versus Weber number, We_2, as a function of Ohnesorge number, Z. Lines, numerical solutions of eqn (3); symbols, curvefit, eqn (5).

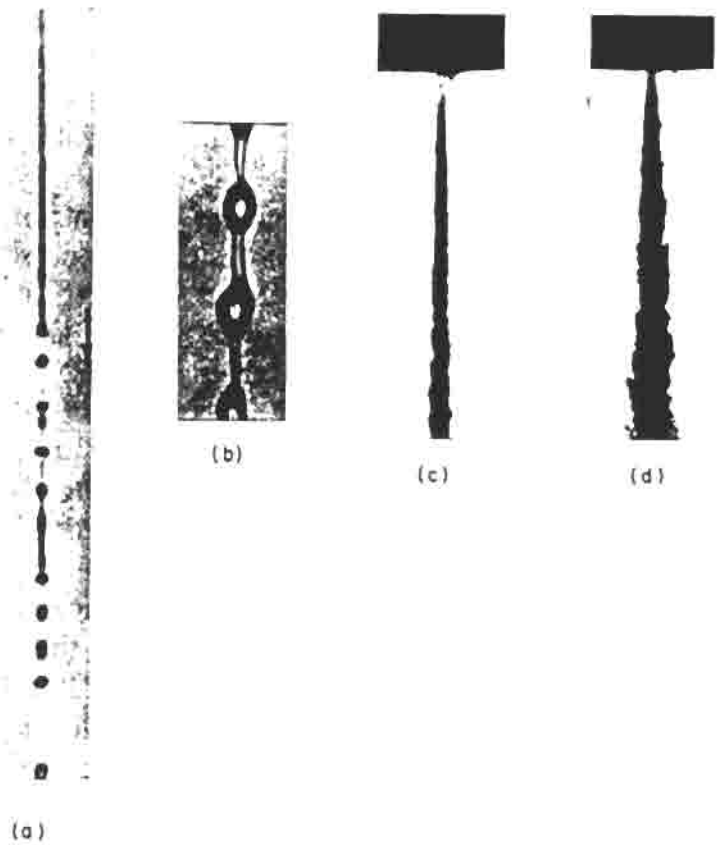

Fig. 4. Examples of jets in the four breakup regimes. (a) Rayleigh regime; drop diameter larger than that of the jet and breakup occurs many nozzle diameters downstream of the nozzle. (b) First wind induced regime; drop diameters of the order of jet diameter and breakup occurs many nozzle diameters downstream of the nozzle. (c) Second wind induced regime; dropsizes smaller than the jet diameter and the breakup starts some distance downstream of the nozzle. (d) Atomization regime; dropsizes much smaller than the jet diameter and the breakup starts at the nozzle exit.

diameter. There is a balance between liquid inertia (the term involving ω^2 on the left hand side) and surface tension (term involving σ on the right hand side) in eqn (3). The jet surface is unstable for all wavenumbers with $ka < 1$ and the maximum growth rate occurs at $\lambda = 9{\cdot}02a$. Inclusion of the liquid viscosity (term involving ν_1 on the left hand side) moves the most unstable wave to longer wavelengths but the jet breakup agency remains the destabilizing combination of surface tension and inertia forces. The liquid viscosity has a secondary stabilizing effect also in the other breakup regimes discussed below.

The inertial effect of the surrounding gas enters as We_2 is increased and the term involving ρ_2 on the right hand side of eqn (3) becomes significant. This enhances the wave growth rate but the dropsizes are still of the order of the jet diameter. However, eqn (3) predicts

unstable waves with wavenumbers extending beyond $ka = 1$ (i.e. shorter waves than for Rayleigh breakup). Notice in eqn (3) that when $ka > 1$, surface tension forces start to oppose the breakup process. This regime has been called the first wind induced breakup regime (Fig. 4(b)).

With further increases in We_2, the gas inertia effect increases. Equation (3) predicts that the maximum growth rate occurs at progressively larger wavenumbers and the breakup is now due to unstable growth of short wavelength surface waves. Drops are formed with sizes much less than the jet diameter (Fig. 4(c)). Solutions to eqn (3) are independent of the jet diameter when We_2 is sufficiently large. Reitz and Bracco[1] call this the second wind induced breakup regime.

A final regime, called the atomization regime in Fig. 4(d), is reached in the high Weber number limit when the gas density is sufficiently high. This is the regime of interest in high-pressure sprays such as in diesel engines. Here breakup commences at the nozzle exit and the spray is conical. Previous studies suggest that the surface wave mechanism of the second wind induced regime could still apply to jets in the atomization regime.[2,4] However, direct verification of this mechanism by means of experiment has not yet been possible because the dense spray which surrounds the jet obscures the breakup details.

3 MODEL

3.1 Computer code

The KIVA computer program solves the three-dimensional equations of transient chemically reactive fluid dynamics, together with those for the dynamics of an evaporating liquid spray. The governing equations and the numerical solution method are discussed in detail by Amsden *et al.*[5] and will be described only briefly.

The conservation laws for gas mass, momentum, internal energy and scalar turbulence variables (k and ε) are solved in KIVA subject to appropriate initial and boundary conditions using a time-marching explicit finite difference numerical method. An acoustic subcycling method is used for computational efficiency at low Mach numbers. Stochastic parcel injection is used for the spray drops. In this technique each computational parcel represents a number or group of physically similar drops and the spray properties at each point in space and time are described by statistically sampling the spray parcels. The drop parcels exchange mass, momentum and energy with the gas through

source terms in the gas equations. KIVA characterizes a spray drop with one size dimension (i.e. as if drops are spheres).

Both three-dimensional and axisymmetric computations were made, the latter to save computer time. A typical computational domain is shown in Fig. 5 (in Fig. 5 the cylindrical domain had radius 30 mm and length 100 mm with 24 radial, 15 azimuthal and 24 axial computational cells). The mesh spacing was non-uniform, with fine resolution on the centerline and close to the injector (the smallest cell was 1 mm wide by 2 mm long). Some 4000 computational drop-parcels were used in the calculations. Numerical experiments with finer meshes and more drops confirmed that results are also grid- and timestep-independent. At the start of each computation the domain consisted of quiescent gas at the desired pressure and temperature. Spray parcels were injected from the center of the top face of the cylinder.

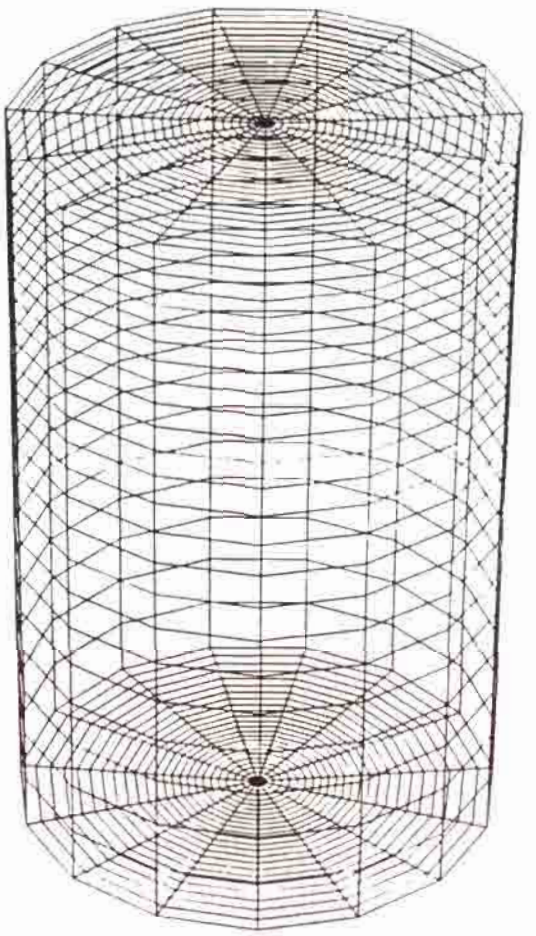

Fig. 5. Typical computational domain. Liquid 'blobs' are injected from the center of the top face of the cylinder.

3.2 Liquid injection

A modification of the method of Reitz and Diwakar[3] was used to describe liquid injection. Parcels of blobs were injected with a characteristic size equal to the nozzle hole diameter, d_0, i.e.

$$D_{\text{init}} = d_0 \tag{6}$$

(mono-disperse injection). The number of blobs injected in unit time was determined from the mass flowrate. The blobs were given an initial radial velocity component, $V_0 = U_0 \tan(\theta/2)$ where the spray angle, θ, was assumed to be uniformly distributed between 0 and Θ where

$$\tan(\Theta/2) = A_1 \Lambda \Omega / U_0. \tag{7}$$

U_0 is the injection velocity given by $c\ (2\Delta P/\rho_1)^{0.5}$ (c is the nozzle discharge coefficient and ΔP is the net injection pressure). Λ and Ω were found from eqns (4) and (5) and A_1 is a constant equal to 0·188 (A_1 depends on nozzle design;[6] the value used here is appropriate for sharp entrance constant diameter tube nozzles with length to diameter ratios of 4–8). This latter method differs from that of Reitz and Diwakar,[3] who determined the spray angle from an experimental correlation, $\tan(\Theta/2) = 0{\cdot}7\ (\rho_2/\rho_1)^{0.5}$ which can be derived from eqns (7), (4) and (5) in the limits $We_2 \to \infty$, and $Z = 0$ (i.e. for high speed inviscid jets).

This blob injection method of prescribing atomization differs from that of earlier studies which assumed that the liquid is already finely atomized at the nozzle exit.[7,8] In those studies an initial distribution of dropsizes is assumed at the nozzle with the Sauter Mean Diameter ($D_{3,2}$) given by the correlation

$$D_{3,2_{\text{init}}} = A_2 \frac{\sigma}{\rho_2 U_0^2} \tag{8}$$

where A_2 is usually taken to be a constant.[4,7,8] The assumption of immediate atomization at the nozzle exit does not account for the presence of a core within a high-pressure spray. Electrical conductivity probe measurements suggest that there is an 'intact core' of largely unbroken liquid which can extend for hundreds of nozzle diameters.[9] Correlations for the length of the core are of the form

$$L = 0{\cdot}5 A_3 d_0 (\rho_1/\rho_2)^{0.5} \tag{9}$$

where the constant A_3 has been given as 14–30.[9]

A core region is predicted with the present blob injection method. This is because the injected blobs breakup due to interaction with the

surrounding gas as they penetrate, yielding a region of relatively large drops near the nozzle. This region of large discrete particles is conceptually equivalent to a core of churning liquid ligaments within the context of a sub-grid-scale model. An attempt to account for the presence of a core has also been made by Chatwani and Bracco.[10] In their method already atomized drops are introduced from a line source which extends downstream of the nozzle within the spray. However it is necessary to assume the extent and location of this source region as a function of time during the injection.

3.3 Liquid breakup

Liquid breakup was modeled by postulating that new drops are formed (with drop radius, r) from a parent drop or blob (with radius, a) with

$$r = \begin{cases} B_0\Lambda & (B_0\Lambda \leq a) \quad (10a) \\ \min \begin{cases} (3\pi a^2 W/2\Omega)^{0.33} \\ (3a^2\Lambda/4)^{0.33} \end{cases} & (B_0\Lambda > a, \quad \text{one time only}) \quad (10b) \end{cases}$$

where B_0 is a constant taken equal to 0·61. In eqn (10a) it is assumed that (small) drops are formed with dropsize proportional to the wavelength of the fastest growing or most probable unstable surface wave (see also Fig. 1). Equation (10b) applies to drops larger than the jet and it assumes that the jet disturbance has frequency $\Omega/2\pi$ (a drop is formed each period) or that dropsize is determined from the volume of liquid contained under one surface wave.

The rate of change of drop radius in a parent parcel of N_0 drops due to drop breakup was described using the rate expression of Reitz and Diwakar,[3]

$$\frac{da}{dt} = -(a - r)/\tau \qquad (r \leq a) \tag{11}$$

where

$$\tau = 3{\cdot}726B_1 a/\Lambda\Omega \tag{12}$$

and $a(t = t_0) = a_0$ is the initial drop radius at time t_0. Equation (12) appears to differ from that used by Reitz and Diwakar[3] but will be seen below to be consistent with their drop breakup time correlations.

In the study of Reitz and Diwakar,[3] the number of drops in the (parent) parcel was increased with time using $Na^3 = N_0 a_0^3$ (to conserve mass) but no new parcels of (product) drops were added to the computations due to breakup. In essence, with their method the product drops are given the same size as the parent drop.

In the present study, a new parcel containing product drops of size r was created and added to the computations when sufficient product drops had accumulated. This was done when the mass of liquid to be removed from the parent ($=\rho_1 4\pi(a_0^3 - a^3)/3$) reached or exceeded 3% of the average injected parcel mass (=total liquid mass injected/total number of parcels) and if the number of product drops was greater than or equal to the number of parent drops. (The numbr of drops in the product parcel was found knowing the parcel mass and dropsize). While waiting for sufficient product drops to accumulate, the parent drop number was adjusted so that $Na^3 = N_0 a_0^3$ (as by Reitz and Diwakar[3]) but the original parent drop number, N_0, was then restored following the creation of the new product parcel.

In the case $B_0\Lambda > a$ (i.e. waves with wavelengths approaching or longer than the characteristic size of the parent blob), the parent parcel was replaced by a new parcel containing drops with size given by eqn (10b) after a time equal to τ (with $N = N_0 a_0^3/r^3$). This 'breakup' procedure was only allowed once for each injected parcel (to prevent product drops from undergoing further unrealistic size increases). Following each breakup event, the product drop parcels were given the same temperature and physical location as the parent. They were given the same velocity (magnitude) as the parent in the direction of the parent drop velocity vector, V. The other velocity components, v and w, normal to V, were given by $v = |V| \tan(\theta/2) \sin\phi$ and $w = |V| \tan(\theta/2) \cos\phi$ where θ is as given in eqn (7), and ϕ was chosen at random on the interval $(0, 2\pi)$.

Predictions of eqn (11) were compared with data of Reinecke and Waldman[11] on the breakup of isolated drops. The symbols in Fig. 6 show their X-ray densitometry measurements of mass loss versus time from (parent) drops in high-relative-velocity flows. (No details were given about the sizes of the product drops stripped from the parent drops). Mass and time were non-dimensionalized by Reinecke and Waldman by the initial drop mass and by $T = 2a_0(\rho_1/\rho_2)^{0.5}/W$. The lines show eqn (11) with various values of B_1 (for these calculations the shed dropsize, r, was assumed to be zero—this gives a linear decrease in parent drop radius with time—and Λ and Ω were determined from eqns (4) and (5) in the limit as $We_2 \to \infty$ and $Z = 0$ (i.e. high speed inviscid liquid breakup)).

The value $B_1 = 10$ was chosen for the present study. It is of interest to consider also experimental data on breakup times of low velocity jets. In this case jet breakup time can be estimated from eqn (1) to be $T = \ln(a_0/\eta_0)/\Omega$ (at this time the height of the most unstable surface wave equals the jet radius) and published values of $\ln(a_0/\eta_0)$ lie in the

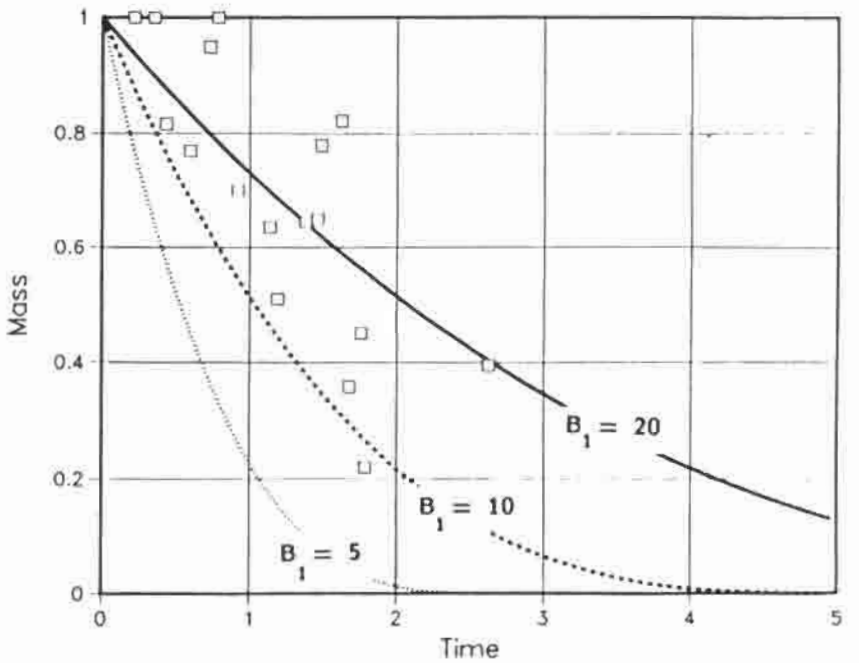

Fig. 6. Non-dimensional mass loss versus time from a drop in a high relative velocity flow. Symbols, experiments of Reinecke and Waldman;[11] lines, drop breakup model, eqn (11), with various values of the drop breakup time constant, B_1.

range 11–16.[12] In the low speed inviscid jet limit ($We_2 = 0$, $Z = 0$), eqn (12) gives $\tau = 0{\cdot}41B_1/\Omega$ so that low velocity jet breakup times are underestimated by a factor of 3 or 4 with $B_1 = 10$. However, it is well known that jet breakup times are influenced by the magnitude of initial disturbance levels to the jet as well as by flow turbulence and nozzle design details.[1,13] Until these effects are quantified, B_1 must be regarded as an adjustable model constant, possibly with a different value in each breakup regime.

It is of interest to compare the above model of liquid breakup with previous breakup models. Reitz and Diwakar[3] introduced eqn (11) to describe the decrease with time of dropsize due to breakup. The drop breakup time, τ, was determined from the minimum of t_1 and t_2, where

$$t_1 = \pi\left[\frac{\rho_1 a^3}{2\sigma}\right]^{0.5} \tag{13a}$$

$$t_2 = B_2 \frac{a}{W}(\rho_1/\rho_2)^{0.5} \tag{14a}$$

where t_1 is the time for bag-type drop breakup (assumed by Reitz and Diwakar[14] to be the inverse of the drop natural frequency) and t_2 is the time for stripping-type breakup given by Nicholls.[15] Reitz and

Diwakar[14] observed that t_2 is usually less than t_1 in high-pressure sprays and the particular regime of breakup was determined from the breakup criteria[15]

$$We_2 > 6{\cdot}0 \qquad \text{(bag breakup)} \tag{15a}$$

and

$$We_2/Re_2^{0{\cdot}5} > 0{\cdot}5 \qquad \text{(stripping breakup).} \tag{16}$$

The breakup times t_1 and t_2 can be derived from eqn (12) in the limit $Z = 0$ (inviscid liquid) using eqns (4) and (5) giving

$$\tau = 1{\cdot}72\, B_1 \left[\frac{\rho_1 a^3}{2\sigma}\right]^{0{\cdot}5}, \qquad We_2 \to 0 \tag{13b}$$

$$\tau = B_1 \frac{a}{W} (\rho_1/\rho_2)^{0{\cdot}5}, \qquad We_2 \to \infty \tag{14b}$$

so that τ agrees with (13a) or (14a) if $B_1 = 1{\cdot}8$ or $B_1 = B_2$ in the two limits, respectively. Reitz and Diwakar[3] used $B_2 = 20$, Nicholls[15] gave $B_2 = 8$ and O'Rourke and Amsden[16] have suggested that $B_2 = \sqrt{3}$ (when this latter value is used in eqn (13b), the drop natural frequency of eqn (13a) is recovered). So there is uncertainty about the value of the breakup time constant.

Reitz and Diwakar[3] used the breakup criterion given by eqn (16) as an equality to determine the equilibrium or stable drop radius, r, in eqn (11) (eqn (15a) was used when $t_1 > t_2$). Interestingly, it has been observed recently by O'Rourke and Amsden[16] and also confirmed in the present study that very similar equilibrium dropsizes result if breakup criterion (15a) is always used to specify r. In fact, O'Rourke and Amsden criticize the use of the breakup criterion of eqn (16) which includes the Reynolds number based on gas properties. The gas viscosity was not varied appreciably by the proposers[17] of the criterion eqn (16), and there appears to be little other justification for its use.

Dropsizes have been measured recently at the edge of high-pressure sprays in the vicinity of the nozzle exit[4] and the data indicate that experimental dropsizes do follow a Weber number correlation such as that of eqn (15a) (see eqn (8)). This is also predicted with the present breakup model, for, in the limit of large We_2 (high speed jet) and $Z = 0$ (inviscid liquid), eqn (10a) gives

$$r = 9{\cdot}8\, B_0 \sigma/\rho_2 W^2 \tag{15b}$$

With $B_0 = 0{\cdot}61$, eqn (15b) is the same as breakup expression (15a) which was used by Reitz and Diwakar[3] and O'Rourke and Amsden[16] to estimate stable or final dropsizes.

3.4 Drop collision and coalescence

The drop collision and coalescence model of O'Rourke and Bracco[8] was used in the computations. Briefly, a collision frequency ν_{12} between drops in parcels 1 and 2 (parcel 1 contains the larger drops) is calculated for all parcels in each computational cell, where

$$\nu_{12} = N_2 \pi (r_1 + r_2)^2 \, |v_1 - v_2| / \mathrm{Vol} \tag{17}$$

N_2 is the number of drops in parcel 2, v is the drop velocity vector and Vol is the volume of the cell. The number of collisions, n, is assumed to follow the Poisson distribution

$$p(n) = e^{-\nu_{12}\Delta t} (\nu_{12}\Delta t)^n / n!$$

where Δt is the computational time step and $p(n)$ is chosen stochastically from the uniform distribution in the interval (0,1).

The outcome of the collision is either a grazing collision (in a grazing collision the colliding drops maintain their sizes and temperatures but undergo velocity changes[8]) or it is coalescence depending on whether the collision impact parameter, b, is greater or less than a critical value,

$$b_{\mathrm{crit}}^2 = (r_1 + r_2)^2 \min (1{\cdot}0, 2{\cdot}4(\gamma^3 - 2{\cdot}4\,\gamma^2 + 2{\cdot}7)/\mathrm{We}_1) \tag{18}$$

and

$$b^2 = q(r_1 + r_2)^2$$

Equation (18) was derived by O'Rourke and Bracco[8] using experimental drop coalescence results of Brazier-Smith *et al.*[18] In the equations q is a random number on the interval (0,1) and $\gamma = r_1/r_2$. If coalescence is predicted, n drops are removed from parcel 2 and the size, velocity and temperature of the drops in parcel 1 are modified appropriately.[8]

Equation (17) was also applied in the present computations to account for collisions and coalescence of the product drops on the scale of the parent drop. For this purpose the collisional volume was assumed to be $\mathrm{Vol} = \pi a^2 \, |v_1 - v_2| \, \delta t$ (i.e. swept volume based on the parent drop area) and δt is the time between shedding of product drops. It was assumed that $r_1 = r_2 = r$, where r is the product drop radius. Significant coalescence of the product drops occurred only when the product dropsize was very much smaller than the parent dropsize (i.e. large We_2).

3.5 Turbulence dispersion and vaporization

The effect of turbulence modulation due to interaction between the spray drops and the gas was modeled in the present study using the

method described by Reitz and Diwakar.[3] With this model the standard equations for the turbulence kinetic energy (k) and the turbulence energy dissipation rate (ε) (see, for example, Ref. 19) are modified to include additional source terms, S and $3\varepsilon S/2k$, respectively, where

$$S = \int f\rho_1 \frac{4}{3}\pi r^3 F \cdot u \, dr \, dv \, dT \tag{19}$$

Here

$$\frac{dv}{dt} = F = \frac{3}{8}\frac{\rho_2}{\rho_1}\frac{|W|}{r} W C_D \tag{20}$$

and C_D is the drop drag coefficient. u represents the fluctuating component of the gas velocity vector due to turbulence and it is specified assuming a Gaussian velocity distribution with zero mean and variance $2k/3$. With this approach, turbulent dispersion of the drops (calculated by integrating eqn (20)) is modeled as a random walk process.[20] The walk durations are calculated from the drop residence time within an eddy or from the eddy lifetime, whichever is smaller, and a new value of u is chosen for each new walk. In eqn (19), f is the number density of drops of size r, velocity v, temperature T in the physical space at time t and $W = |U + u - v|$ is the relative velocity between the drop and the gas (U is the gas mean velocity vector).

The rate of drop radius change due to vaporization was given by the Frossling correlation[21]

$$\frac{dr}{dt} = -\rho_2 DB \, \mathrm{Sh}/(2\rho_1 r) \tag{21}$$

where Sh is the Sherwood number, B is the mass transfer number, D is the mass diffusivity of fuel in air. The fuel mass fraction at the drop surface (which appears in B) was obtained by assuming that the partial pressure of fuel vapor is equal to the equilibrium vapor pressure at the drop temperature T_1. The drop temperature change with time was obtained from an energy balance involving the latent heat of vaporization and heat conduction from the gas. The rate of heat conduction to the drop, Q, was modeled with the correlation[21]

$$\mathrm{Q} = \alpha(T_2 - T_1)\,\mathrm{Nu}/(2\rho_2 r)$$

where Nu is the Nusselt number, T_1 and T_2 are the drop and gas temperatures, respectively, and α is the thermal diffusivity. Tabulated data was used to describe thermodynamic properties of the liquid and gas as functions of temperature, pressure and composition. These and other details of the drop vaporization model are discussed in detail by Amsden *et al.*[5]

4 RESULTS AND DISCUSSION

4.1 Jet breakup regimes

Figure 7(a)–(c) shows computational results for jets 2·4 ms after the beginning of injection. Figure 7(d) shows a jet 12·0 ms after the start of its injection. The injector is oriented vertically downward in each diagram. The injection velocity was 40 m/s, the nozzle diameter was 0·2 mm and the liquid and gas temperature was 298 K in each case. The spray liquid was tetradecane ($\rho_l = 770$ g/liter, $\sigma = 21{\cdot}8$ g/s^2, $\nu_l = 2{\cdot}5$ mm^2/s). The only quantity varied was the air pressure (density) which was 50, 200, 500 and 2500 kPa for Fig. 7(a), (b), (c) and (d), respectively.

Unbroken injected liquid blobs are shown as solid circles. The even spacing between blobs (which is seen clearly in Fig. 7(a)) reflects the present discrete blob injection method. Spray parcels are produced from the breakup of these blobs and the parcel locations are shown as

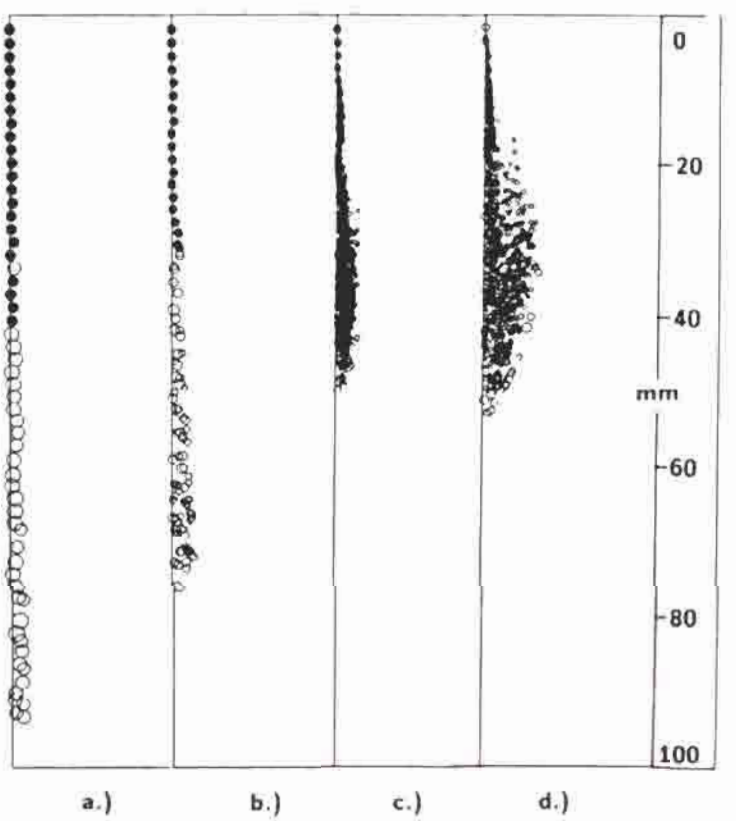

Fig. 7. Predictions of jet breakup regimes. (a) $We_2 = 4{\cdot}5$; (b) $We_2 = 18{\cdot}1$; (c) $We_2 = 45$; (d) $We_2 = 226$. Axisymmetric computations, sprays (a), (b) and (c) shown at 2·4 ms after the beginning of injection, spray (d) at 12 ms. ●, unbroken injected liquid blobs; ○, drops (dropsize is proportional to size of the circles in each figure).

open circles. The size of each circle is proportional to the size of the drops in the parcel (of course, dropsize is exaggerated greatly in the figures and the number of spray drops in each parcel is not shown).

In Fig. 7(a) ($We_2 = 4{\cdot}5$), the liquid blobs break up only after a long intact length and the dropsizes are larger than the original jet (blob) diameter as in Rayleigh's breakup regime. The jet tip penetration is 97 mm which is close to the product of the injection velocity and the elapsed time (i.e. the jet penetrates like a solid rod). In Fig. 7(b) ($We_2 = 18{\cdot}1$), the jet breaks up sooner and the resulting drops are smaller than those of Fig. 7(a), as for a jet in the first wind induced regime of breakup. Jet tip penetration is less than for the jet in Fig. 7(a) due to increased momentum transfer between the jet and the ambient air.

A short intact (unbroken) region of the jet can still be seen close to the nozzle exit in the spray of Fig. 7(c) ($We_2 = 45$). Further downstream drops are produced with sizes much smaller than the nozzle diameter as expected for a jet in the second wind induced jet breakup regime. The jet tip penetration is reduced further due to the increased gas density. Finally, in Fig. 7(d) ($We_2 = 226$), there is no longer any evidence of unbroken liquid near the nozzle and the spray drops are smaller than the nozzle diameter as for a jet in the atomization regime. The spray penetration is reduced considerably (Fig. 7(d) is at 5 times the gas density and 5 times the elapsed time of the spray of Fig. 7(c)). The radial spread of the high gas density spray is also larger than that of Fig. 7(c) as would be expected.[6]

4.2 Structure of high-pressure sprays

To study the structure of atomizing jets comparisons were made with measurements of Hiroyasu and Kadota[22] of spray tip penetration and dropsize. The test conditions are given in Table 1 ($D_{3,2}$ is the average over the spray cross-section 65 mm downstream of the nozzle). The

TABLE 1
Test Conditions for the Measurements of Hiroyasu and Kadota[22]

Case	P_2 (MPa)	V_0 (m/s)	$D_{3,2}$ (μm)
1	1·1	102·0	42·4
2	3·0	90·3	49·0
3	5·0	86·4	58·8

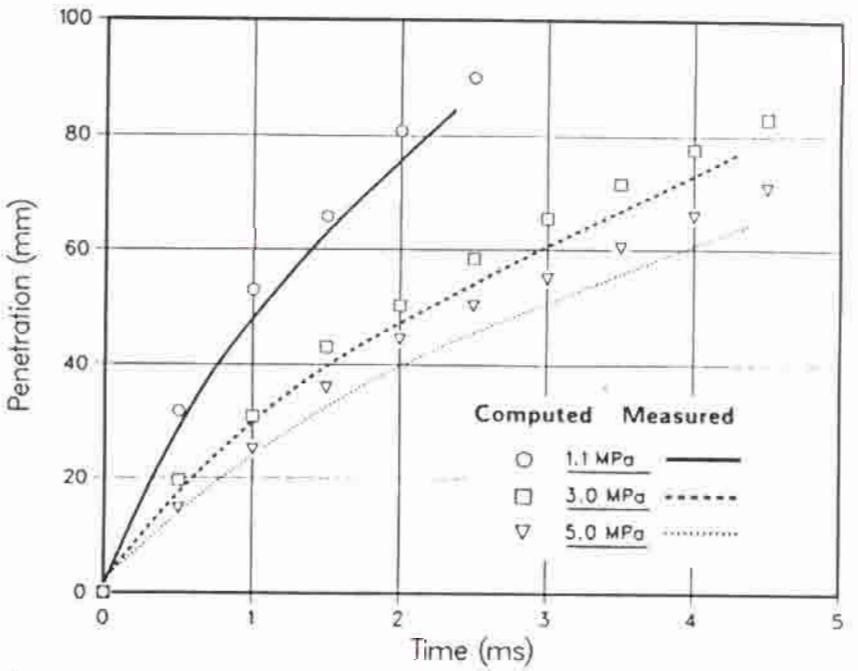

Fig. 8. Spray tip penetration versus time for the sprays of Table 1. Lines, measurements of Hiroyasu and Kadota;[22] symbols, present computations.

nozzle diameter was 0·3 mm and the computations used tetradecane for the spray liquid (the experiments used a diesel fuel oil with physical properties close to tetradecane) and the liquid and gas temperature was 298 K.

The lines in Fig. 8 show the measured spray tip penetrations for the three sprays of Table 1. The symbols indicate computed results with the present model. It is seen that there is good agreement between the model and the measurements although the calculated penetration is slightly higher in all three cases. This could be attributed to imprecise definition of the spray tip. In the calculations the spray tip was defined to be the location of the leading spray drop parcel. Other definitions are possible[23] but they give similar magnitudes for penetration. Previous studies have shown that spray penetration is influenced mostly by the turbulence diffusivity[3] and the present good agreement indicates that the turbulence is computed accurately.

Figure 9 shows the variation of drop Sauter Mean Diameter with axial distance from the injector. The open symbols connected by lines are the model results and the three solid data points at 65 mm are the measurements. The computed dropsize is a time average (for 4·5 ms) over the spray cross-section at each axial station. At the nozzle exit the drop diameter is equal to the nozzle size (nozzle diameter is 0·3 mm). Due to drop breakup, dropsize decreases rapidly within a short distance

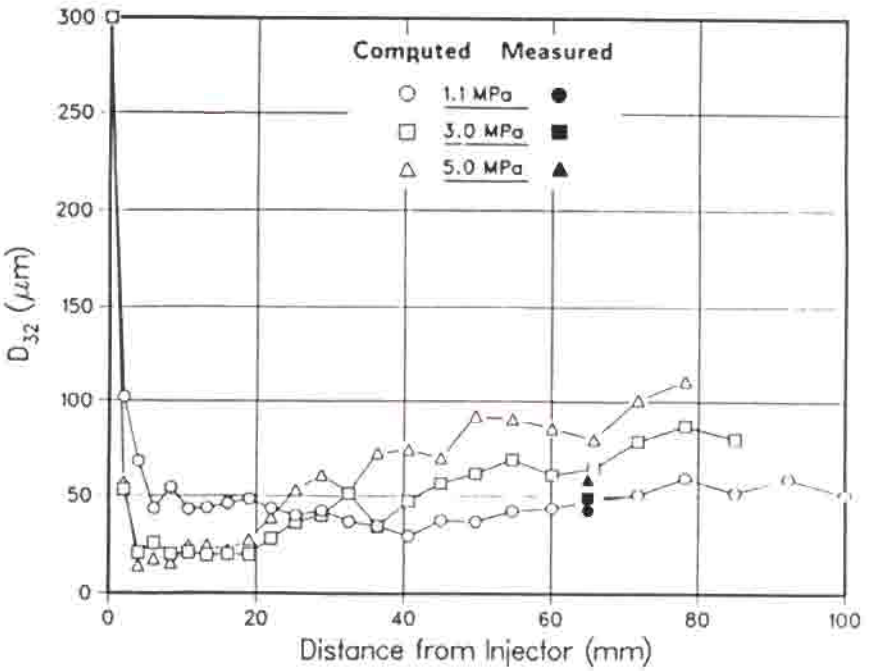

Fig. 9. Sauter Mean Diameter variation with distance from the nozzle for the sprays of Table 1. Solid data points at 65 mm measurements of Hiroyasu and Kadota;[22] open symbols, present computations.

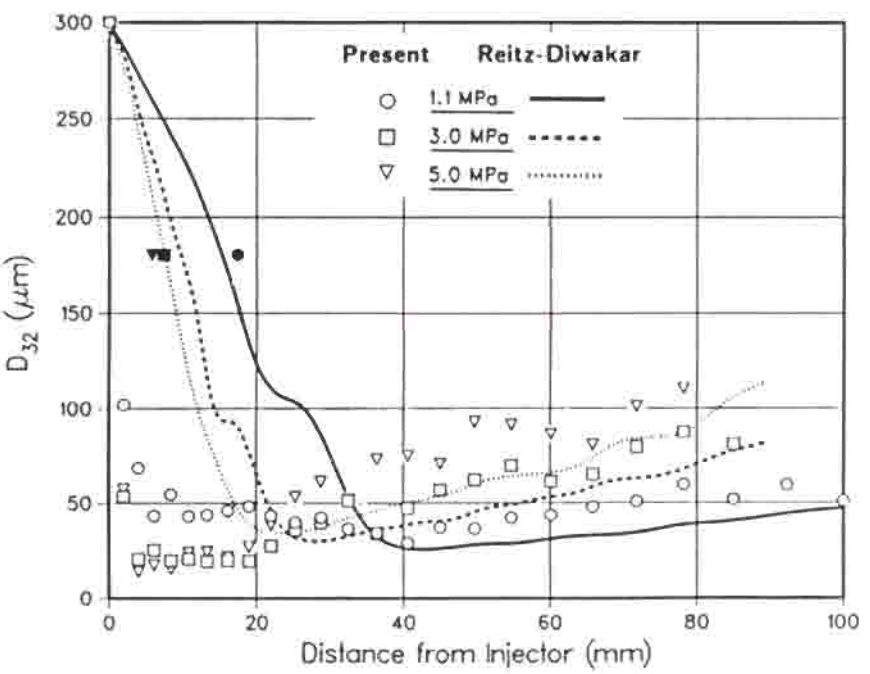

Fig. 10. Sauter Mean Diameter variation with distance from the nozzle for the sprays of Table 1. Open symbols, present computations; lines, computations with the breakup model of Reitz and Diwakar[3] which does not account for small product drops in the core near the nozzle; solid symbols, core length estimates from Fig. 11.

from the nozzle and then gradually increases. In the low gas pressure (density) case (1·1 MPa) the dropsize remains fairly uniform after the initial region; higher gas densities promote collisions and coalescences (and breakups) yielding larger downstream dropsizes. This trend is also evident in the measurements but the predicted dropsizes for the high pressure cases are somewhat larger than the measured values.

It is interesting to compare the above dropsize results which are repeated in Fig. 10 with results (shown by the lines) obtained with the drop breakup model of Reitz and Diwakar[3] which does not distinguish between product and parent drops. Far downstream of the nozzle the two studies give dropsizes and trends that are similar. This confirms that eqn (15a) (used by Reitz and Diwakar[3]) and eqn (16) (effectively used in the present study) predict similar equilibrium or stable dropsizes. This has also been found by O'Rourke and Amsden.[16]

However, large differences in the computed Sauter Mean Diameters are seen in the core region near the nozzle for the two sets of

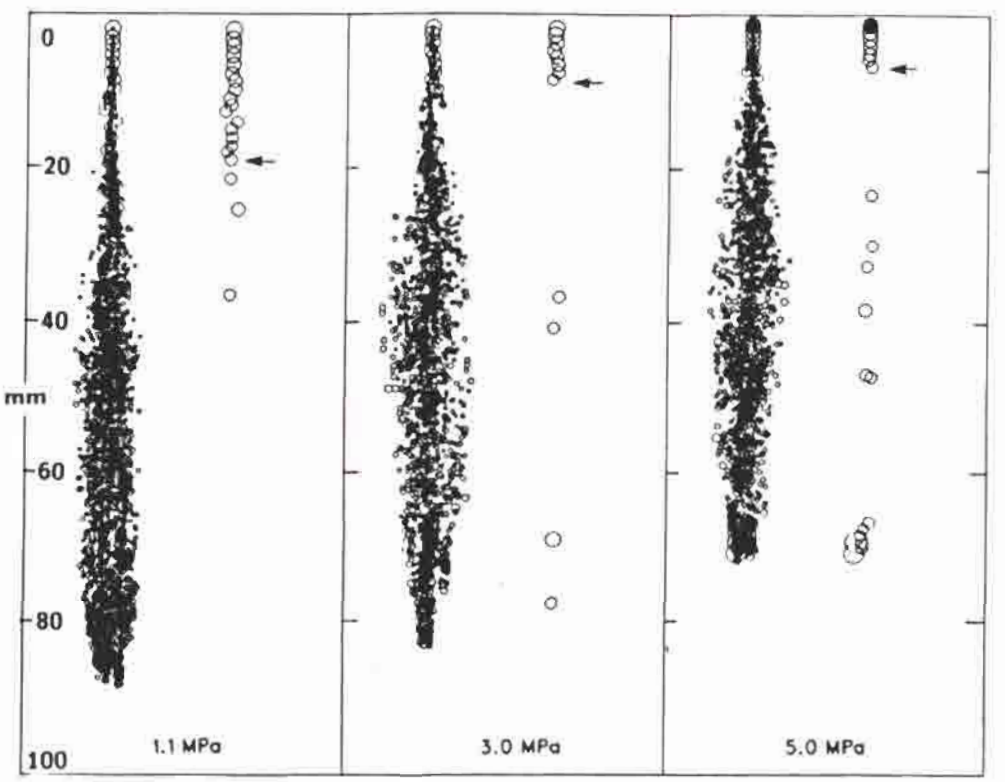

Fig. 11. Spray parcel plots showing co-existing large drops and small product drops in the core region near the nozzle. Plots at the top of each frame show only the parcels containing drops with diameters larger than 180 μm. The appearance of large drops downstream of the core is due to drop coalescence. Spray conditions given in Table 1. 1·1 MPa case shown at 2·5 ms, 3·0 and 5·0 MPa cases shown at 4·5 ms after start of injection.

calculations. The explanation is that the breakup model of Reitz and Diwakar does not account for the presence of the finely atomized product drops which are predicted to co-exist with the large drops in the core. These small drops increase the spray drop surface area dramatically and this leads to much smaller values of $D_{3,2}$.

The fact that these large drops are present in the core of sprays computed with the present drop breakup model is shown in Fig. 11 which plots spray parcel locations for the three sprays (2·5 ms after the start of the injection for the 1·1 MPa case and at 4·5 ms for the 3·0 and 5·0 MPa cases). A corresponding plot showing only those parcels with drops larger than 180 μm diameter is presented at the top of each figure. These plots show that the core length decreases with increasing gas density consistent with the experimental correlation, Eqn (9). The arrows indicate the point chosen to represent the position of the last 180 μm drops in the core. These points are also plotted in Fig. 10 with the solid symbols. It is seen that the present core lengths agree quite well with the core locations of Reitz and Diwakar.[3] Large drops are also found downstream of the core in Fig. 11. They reflect the effect of drop coalescences which increases as the gas density is increased.

4.3 High-pressure spray vaporization

Computations were made of high-pressure vaporizing sprays and the results were compared with recent experimental results of Heinze and Daams[24] who measured equivalence ratio distributions within n-heptane sprays using spontaneous Raman spectroscopy. In the study the nozzle diameter was 0·2 mm, the air temperature and pressure were 773 K and 4·5 MPa, respectively, and the injection velocity was about 160 m/s. More details of the experimental technique and apparatus are also given in Scheid *et al.*[25]

Figure 12 shows computed equivalence ratio contours at 2·4 ms after the start of the injection using the present drop breakup model (Fig. 12(a)) and using the model of Reitz and Diwakar[3] (Fig. 12(b)) (equivalence ratio is defined as the fuel–air mass ratio divided by the stochiometric one). The two sets of computed results can be seen to be qualitatively different in the region near the nozzle. Further downstream the results are more similar. The computed spray parcel locations are also shown at the left of each figure. The spray tip penetration differs by only about 10% in the two cases (tip location is at 75 mm in Fig. 12(a) and 82 mm in Fig. 12(b)). The axial penetration of fuel vapor is also slightly larger with the breakup model of Reitz and Diwakar (Fig. 12(b)).

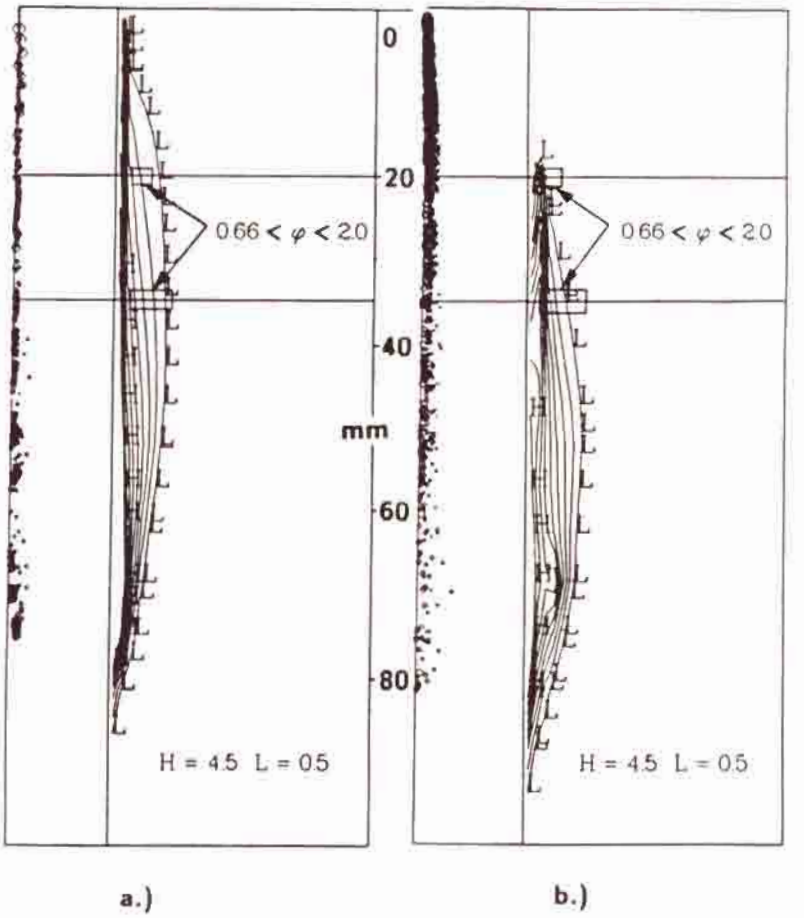

Fig. 12. Computed equivalence ratio contours (ϕ) at 2·4 ms after start of injection. (a) Present drop breakup model which accounts for small product drops in the core; (b) drop breakup model of Reitz and Diwakar[3] which predicts only large drops in the core. Low contour (L), $\phi = 0{\cdot}5$, high contour (H), $\phi = 4{\cdot}5$. Measured 'ignitable' regions of Heinze and Daams[24] indicated by the arrows. Liquid n-heptane, air temperature 773 K, air pressure 4·5 MPa.

The data of Heinze and Daams[24] are indicated by the arrows in the figures. They presented measurements of the radial extent of 'ignitable' regions of the spray. These are shown by the boxes in Fig. 12 at 20 mm and 35 mm downstream of nozzle. 'Ignitable' regions were defined as regions where the equivalence ratio is in the range $0{\cdot}66 < \phi < 2{\cdot}0$. An examination of Fig. 12(a) reveals that significant fuel vaporization is predicted starting immediately at the nozzle exit. This is due to the presence of the small product drops which are formed from the atomizing jet and which vaporize rapidly (there is no evidence of an unbroken region near the nozzle in the spray of Fig. 12(a)). The location of the computed equivalence ratio contours is in good agreement with the measured ignitable region at 20 mm downstream of

the nozzle. At 35 mm, the width of the region of ignitable fuel vapor in the measurements extends radially outside the predicted contours slightly, but there is still good qualitative agreement between the experiments and the computations.

The computations of Fig. 12(b) used the drop breakup model of Reitz and Diwakar[3] in which the product drops are given the same sizes as the parent drops. In this case only large drops are found in the core near the nozzle and the drops vaporize slowly yielding negligible vaporized fuel. The predicted radial distribution of vaporized fuel at the 20 mm station is much narrower than that of the measurements. By 35 mm, in the computations, the radial penetration of fuel vapor has increased significantly due to the effect of drop breakup downstream of the core. This breakup yields small downstream drops and small drops have high vaporization rates. However, the predicted vapor distribution still underestimates the radial extent of the measurements.

The corresponding predicted dropsizes are shown in Fig. 13 for the two different breakup models ($D_{3,2}$ is averaged over the spray cross-section). As discussed earlier, the present drop breakup model gives small drops starting at the nozzle exit and the increased surface area of the drops leads to enhanced vaporization rates (and to reduced $D_{3,2}$ values). With the model of Reitz and Diwakar[3] small drops are only found starting downstream of the core. In both models coalescence,

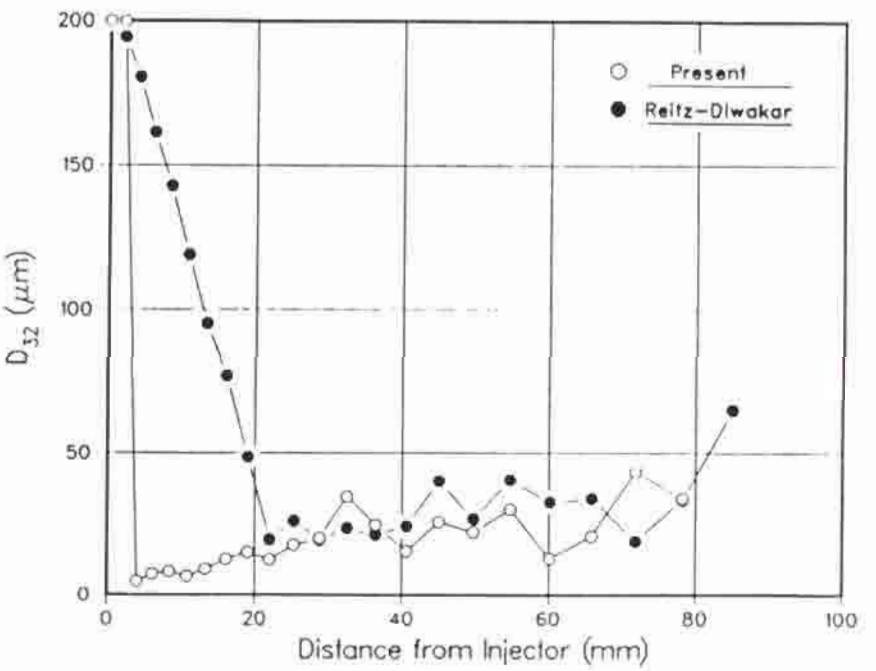

Fig. 13. Sauter Mean Diameter variation with distance from the nozzle for the sprays of Fig. 12.

breakup and vaporization of the drops continues beyond the core. The fact that the two sprays have different dropsizes near the nozzle and yet have similar downstream dropsizes (see Fig. 13) indicates that the downstream dropsize is determined by local drop coalescence, breakup and vaporization rates. This also explains the fact that the fuel vapor distributions which were qualitatively different near the nozzle were found to be similar for the two models far downstream of the nozzle (see Fig. 12(a) and (b)).

5 SUMMARY AND CONCLUSIONS

A new liquid breakup model has been developed that predicts the presence of finely atomized drops which are seen at the spray edge near the nozzle in photographs of high-pressure sprays. The model also predicts an inner core of largely unbroken liquid. This core region has been observed recently with measurements of electrical conductivity within high-pressure sprays. The new model has the added advantage that it also predicts jet breakup details in other (low-pressure) breakup regimes.

The liquid is injected as discrete parcels of drops or 'blobs'. As the blobs break up, new parcels containing product drops are added to the computations and the product drops themselves can undergo further breakups. The size of the new product drops is assumed to be related to the wavelength of unstable waves on the blob's surface.

The small product drops which are predicted by the model in high-pressure sprays have a large surface area and vaporize rapidly. This leads to computed fuel vapor distributions near the nozzle that agree well with recent vapor measurements. Previous drop breakup models that accounted only for large drops near the nozzle predict negligible vaporized fuel in the core region, disagreeing with the measurements.

Downstream of the core, the dropsize is found to be determined by a competition between drop breakup, drop coalescence and vaporization effects. Here too, the new model predicts dropsize and vapor concentrations that agree well with experimental data.

There are aspects of the model that could be refined in future studies. It is assumed that liquid ligaments near the nozzle can, like drops, be described using only one characteristic size dimension. In the absence of experimental data in the core of high-pressure sprays, it is not clear whether more shape detail is necessary. A second point to note is that the stability theory used in the model to predict dropsize does not

predict size distributions or the time between successive breakups. Model constants are introduced in the present study to describe these quantities. The effect of different operating conditions on the values of the constants should be assessed with additional comparisons with experiment.

ACKNOWLEDGMENTS

The author thanks Roger Krieger and Peter O'Rourke for helpful comments.

REFERENCES

1. Reitz, R. D. and Bracco, F. V., Mechanisms of breakup of round liquid jets. In *Encyclopedia of Fluid Mechanics*, Gulf Pub., NJ, **3** (1986) 233–49.
2. Reitz, R. D. and Bracco, F. V., Mechanism of atomization of a liquid jet. *The Physics of Fluids*, **25** (1982) 1730–42.
3. Reitz, R. D. and Diwakar, R., *Structure of high-pressure fuel sprays*, SAE Paper 870598, 1987.
4. Wu, K.-J, Reitz, R. D. and Bracco, F. V., Measurements of drop size at the spray edge near the nozzle in atomizing liquid jets, *The Physics of Fluids*, **29** (1986) 941–51.
5. Amsden, A. A., Ramshaw, J. D., O'Rourke, P. J. and Dukowicz, J. K., *KIVA: a computer program for two- and three-dimensional fluid flows with chemical reactions and fuel sprays*, Los Alamos Report No. LA-10245-MS, February 1985.
6. Reitz, R. D. and Bracco, F. V. *On the dependence of spray angle and other spray parameters on nozzle design and operating conditions*, SAE Paper 790494, 1979.
7. Martinelli, L., Bracco, F. V. and Reitz, R. D., *Progress in Astronautics and Aeronautics*, **95** (1984) 484–512.
8. O'Rourke, P. J. and Bracco, F. V., *Modeling of Drop Interactions in Thick Sprays and Comparison with Experiments*, Institution of Mechanical Engineers, 1980, 101–16.
9. Chehroudi, B., Chen, S. H., Bracco, F. V. and Onuma, Y., *On the intact core of full-cone sprays*, SAE Paper 850126, 1985.
10. Chatwani, A. U. and Bracco, F. V., Computation of Dense Spray Jets, *Proc. Int. Conf. on Liquid Atomisation and Spray Systems* (ICLASS-85), Eisenklam, P. and Yule, A. Eds., Institute of Energy, London, U.K., 1985.
11. Reinecke, W. G. and Waldman, G. D., *A study of drop breakup behind strong shocks with applications to flight*, AVCO Report AVSD-0110-70-RR, May 1970.
12. Meister, B. J. and Scheele, G. F., *A.I.Ch.E. J.*, **15** (1969) 689–95.
13. Phinney, R. E., *A.I.Ch.E. J.*, **18** (1972) 432–44.
14. Reitz, R. D. and Diwakar, R., *Effect of drop breakup on fuel sprays*, SAE Paper 860469, 1986.

15. Nicholls, J., Stream and droplet breakup by shock waves, In NASA SP-194, *Liquid Propellant Rocket Combustion Instability*, Eds D. T. Harrje and F. H. Reardon, 1972, 126–8.
16. O'Rourke, P. J. and Amsden, A. A., *The TAB method for numerical calculations of spray droplet breakup*, SAE Paper 872089, 1987.
17. Rabin, E., Schallenmuller, A. R. and Lawhead, R. B., *Displacement and shattering of propellant droplets*, AFOSR TR 60–75, 1960.
18. Brazier-Smith, P. R., Jennings, S. G., and Latham, J., *Proc. R. Soc. Lond. A*, **326** (1972) 393–408.
19. El Tahry, S. H., *J. Energy*, **7** (1983) 345–53.
20. Dukowicz, J. K., *J. Computational Physics*, **35** (1980) 229–53.
21. Faeth, G. M., *Progress in Energy and Combustion Science*, **9** (1983) 1–13.
22. Hiroyasu, H. and Kadota, T., *Fuel droplet size distribution in diesel combustion chamber*, SAE Paper 740715, 1974.
23. Kuo, T.-W. and Bracco, F. V., *Computations of drop sizes in pulsating sprays and of liquid core length in vaporizing sprays*, SAE Paper 820133, 1982.
24. Heinze, Th. and Daams, H.-J., *Measurement of mixture formation in an n-heptane fuel spray by spontaneous raman spectroscopy*, SAE Paper 870098, 1987.
25. Scheid, E., Pischinger, F., Knoche, K. F., Daams, H.-J., Hassel, E. P. and Reuter, U., *Spray combustion chamber with optical access, ignition zone visualization and first raman measurements of local air-fuel ratio*, SAE Paper 861121, 1986.